

Technical report 23-019

Dynamic optimization for minimal HVAC demand with latent heat storage, heat recovery, natural ventilation, and solar shadings*

L.A. de Araujo Passos, P. van den Engel, S. Baldi, and B. De Schutter

If you want to cite this report, please use the following reference instead:

L.A. de Araujo Passos, P. van den Engel, S. Baldi, and B. De Schutter, “Dynamic optimization for minimal HVAC demand with latent heat storage, heat recovery, natural ventilation, and solar shadings,” *Energy Conversion and Management*, vol. 276, p. 116573, 2023. doi:[10.1016/j.enconman.2022.116573](https://doi.org/10.1016/j.enconman.2022.116573)

Delft Center for Systems and Control
Delft University of Technology
Mekelweg 2, 2628 CD Delft
The Netherlands
phone: +31-15-278.24.73 (secretary)
URL: <https://www.dcsc.tudelft.nl>

* This report can also be downloaded via https://pub.bartdeschutter.org/abs/23_019.html

Dynamic optimization for minimal HVAC demand with latent heat storage, heat recovery, natural ventilation, and solar shadings

Luigi Antonio de Araujo Passos^a, Peter van den Engel^b, Simone Baldi^{a,c,*},
and Bart De Schutter^a

^a Delft Center for Systems and Control, Delft University of Technology, Netherlands

^b Architectural Engineering & Technology, Delft University of Technology, Netherlands

^c School of Mathematics, Southeast University, Nanjing, China

Abstract

Satisfying thermal comfort in indoor spaces is still a challenge in terms of energy saving, and several HVAC (Heating, Ventilation, and Air-Conditioning) systems have been proposed for this purpose. This paper conducts an analysis to evaluate and optimize the long-term operation of a novel HVAC system installed at The Green Village, a living lab in Delft, the Netherlands. This system comprises all-glass facades with steerable solar shades, sky windows, a climate tower equipped with Phase-Change Material (PCM), a heat recovery unit, and a heat pump. The current analysis draws on transient modeling to predict the system's behavior while relying on constrained nonlinear optimization to select the optimal design parameters (e.g., floor heat capacity and solar absorptance) and optimal operational conditions (e.g., use of PCM and heat recovery unit, aperture of sky windows and solar shadings). The goal is to schedule the control inputs to operate the system as much as possible as a passive energy system, with minimal active power all year round. The results show that the optimization can reduce the yearly heat demand by around 10.6%, with the solar shadings being the most significant component to be optimized. Furthermore, the optimized system is capable to supply 58% of the annual thermal demand passively – In this case, an auxiliary thermal demand of only 27 kWh/m²/year is required, which may qualify the system as a low-energy building.

Keywords: Indoor climate, natural ventilation, solar shadings, Phase-Change Material (PCM), low-energy buildings, optimization.

*Corresponding Author: S. Baldi, E-mail: s.baldi@tudelft.nl

Nomenclature		τ	Solar transmittance [-]
		φ	Cross-sectional area [m ²]
A	Heat transfer area [m ²]	<i>Subscripts</i>	
c	Specific heat [J kg ⁻¹ K ⁻¹]	a	Air
C_d	Discharge coefficient [-]	as	Active system
g	Gravitational acceleration [m s ⁻²]	$a,0$	Air outside the building
h	Convective heat transfer coefficient [W m ⁻² K ⁻¹]	$a,1$	Air downstream the heat recovery
h	Specific enthalpy [J/kg]	$a,2$	Air downstream the PCM battery
H	Height of the sky windows [m]	$a,3$	Air downstream the mixing unit
I	Solar radiation [W m ⁻²]	$a,4$	Air downstream the active system
k	Thermal conductivity [W m ⁻¹ K ⁻¹]	$a,5$	Air downstream the floor deck
K	Conductive heat transfer coefficient [W m ⁻² K ⁻¹]	$a,6$	Air downstream the building hall
L	Specific latent heat [J kg ⁻¹]	b	Beam radiation
L_c	Characteristic length [m]	bn	Beam normal
N	Time horizon [-]	c	Ceiling or sink
P	Number of people [-]	d	Diffuse and deck floor
P_1-P_3	Coefficients of the Perez model [-]	dh	Diffuse at the horizontal plane
q	Heat [J]	f	Concrete floor
T	Temperature [K or °C]	g	Ground
t	Time [h]	gen	Internal generation
x	Controlling fraction [-]	h	Horizontal
y	Liquid fraction [-]	l	Liquid state
<i>Greek letters</i>		p	PCM
α	Solar absorptance [-]	r	Roof and heat recovery
β	Tilt angle [°]	s	Solar shadings
γ	Optimization parameter [-]	sj	Internal surface
ε	Emissivity [-]	sky	Sky
η	Efficiency [-]	w	Sky windows
θ	Angle of incidence [°]	w_1-w_3	Layers of wall
ξ	Reflectance of the ground [-]	<i>Superscripts</i>	
ρ	Specific mass [kg m ⁻³]	k	Time step
σ	Stefan-Boltzmann constant [W m ⁻² K ⁻⁴]		

1 Introduction

Sustainable urbanization has become a major global concern, which affects the design and the role of the built environment [1]. In terms of HVAC (Heating, Ventilation, and Air-Conditioning), on the one hand, indoor spaces must operate at levels of temperature and humidity collectively suitable [2], with sufficient air renewal [3]. Indeed, lack of air renewal may aggravate several respiratory diseases such as asthma, respiratory infections, and lung infections [4], not to mention recently studied connections between air quality and transmission of SARS-CoV-2 [5, 6]. On the other hand, a crucial sustainability dilemma arises in indoor spaces since the higher the air renewal rates, the higher the energy demand required for air-conditioning [7]. To address this dilemma, several HVAC systems have been designed to make use of passive energy technologies, energy-efficient processes, and renewable energy sources as much as possible [8].

While daylighting and natural ventilation are popular passive technologies for warm and humid climates [9], in cold climates conventional HVAC systems are still promoted, where most designs have considered heat pumps and a variety of batteries for energy storage. For instance, [10] suggests the integration of geothermal heat pumps and electric batteries using Sweden as a reference case. The authors of [11] conclude that in Denmark the use of photovoltaic-thermal-cooling panels provides a better cost-effective scenario than heat pumps and electric batteries. Nonconventional batteries that have been studied include hybrid storage (heat, ice, and electricity) [12], and combined mechanical and thermal storage [13]. Phase-Change Material (PCM) has been often adopted for low-energy purposes [14], including applications like short-term storage [15], air pre-heating [16], and heat recovery [17]. Solar shadings are also a popular option for low-energy buildings [18]. Solar shades have shown optimized performance when operated by dynamic controllers [19], which may consider parametric maps [20], and machine learning algorithms [21].

While choosing the proper combination of technologies depends on the corresponding climatic zone, the optimization of both design parameters and dynamic operation parameters is certainly beneficial when integrating different HVAC systems in dynamic conditions since it can deal with issues such as managing different system actuators simultaneously and making real-time adjustments while satisfying the desired conditions with minimal energy use. The literature has covered several strategies regarding this research gap for the design and optimization of renewable energy systems for low-energy buildings [23] which may rely

on genetic algorithms [24], big bang-big crush algorithm [25], Pareto [26], and grey wolf optimization [27]. Linear programming [28], quadratic programming [29], and particle swarm optimization [30] have also been considered for time-dependent energy management processes such as heat storage in large-scale buildings [31], energy distribution in the neighborhood [32], operation of lighting, shadings, and air-conditioning systems [33], and latent heat storage [34]. Furthermore, genetic algorithms have been combined with artificial neural networks for optimization in buildings, which involves training data for the predictive control [35]. While the system dynamics and the performance indicators determine the best corresponding optimization method, model-based predictive control is particularly effective for dealing with dynamically changing inputs, outputs, and constrained situations [36]. Indeed, such a predictive approach allows an integrated approach where the system variables are optimized simultaneously and may benefit several complementary analysis [37], including air-conditioning with humidification [38, 39] and disease transmission in indoor spaces [40].

In this paper, we consider multi-variable constrained optimization for optimal integration of passive energy sources in order to minimize the demand of the active source. This analysis is motivated by the facilities of The Green Village, which is a living lab in Delft, the Netherlands, for testing sustainable innovation in the built environment. The facility’s uniqueness relies on its lightweight building, fully glazed facades with a glazing/floor space ratio of 120%, and HVAC system comprising dynamic solar shading, PCM buffering for pre-air conditioning, and a heat recovery unit. To the best of our knowledge, the design of optimal parameters and optimal energy management in fully glazed-wall designs are largely open in the literature. The present study addresses these open problems and brings up as novelty the following contributions:

- Developing a modeling approach for the integrated system simulation while deploying the sensors installed in the real facilities to validate the models we propose. To the best of our knowledge, no modeling approach for such complex and novel system was ever reported in the literature.
- Performing a dynamic optimization for both the design and the operational parameters, providing optimal inputs for operating the HVAC simultaneously (i.e., floor properties, air temperatures and airflow, and hourly schedule for shadings, PCM, and sky windows). Again, we are not aware of a similar dynamic optimization approach for such a complex and novel system being reported in the literature.
- Evaluating the long-term performance of the optimized system, which reflects the goals and the effects of the optimization of passive energy systems.

The analyses show that the optimization of technologies can decrease by 10.6% the yearly demand for air-conditioning, which guides new configurations, optimal controllers, and further experimental tests. Moreover, the system proves to be able to supply 58% of the annual demand passively: the annual demand to be provided actively is only 27 kWh/m²/year, which qualifies the system as a low-energy building.

This paper is organized as follows. The system description and numerical modeling are included in Section 2. In Section 3, we formulate the optimization problem to find the optimal parameters. In Section 4 we investigate the optimal long-term performance of the system. After discussing the results, Section 5 presents the conclusions.

2 System description and numerical modeling

The thermal system recently installed in The Green Village considers an innovative integration of a fully glazed walls structure with external steerable solar shades and sky windows, as illustrated in Figure 1. This structure is connected to a climate tower that provides climatization through the combination of a heat recovery unit, a battery of PCM plates, and an active system, as shown in Figure 2a.

The building consists of a rectangular 13.5 m × 5.2 m × 22.5 m glass structure, in which external dynamic shades control the solar heat gains while letting natural light enter the building. The glazed walls prevent heat losses through a 0.01 m-thick triple-glass layer. Moreover, the deck allows the air to come inside the building through a porous surface. The deck is composed of a 0.038 m-thick tile with 0.5 mm diameter holes. Note that the top of the building includes four sky windows for natural ventilation with a cross-sectional area of 3 m² each. While the fans in the climate tower ventilate the building, the heat recovery unit recovers the waste heat from the air downstream of the building, and the PCM battery buffers the oscillations of the temperature of the supply air upstream the building. The active system is only activated when the required indoor conditions cannot be fully supplied by all the other components, here defined as the passive energy system. Table 1 summarizes the system dimensions and properties considered for the building, while Table 2 lists the parameters considered for the PCM battery in the climate tower.

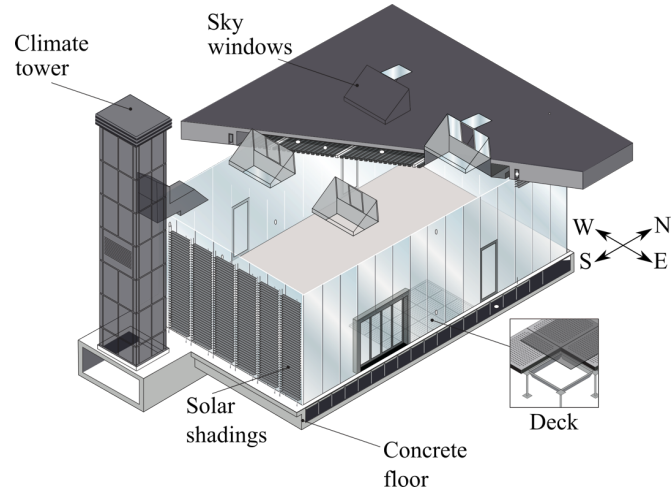


Figure 1: Building configuration with glazed facades, dynamic solar shades, deck and concrete floor, sky windows, and climate tower.

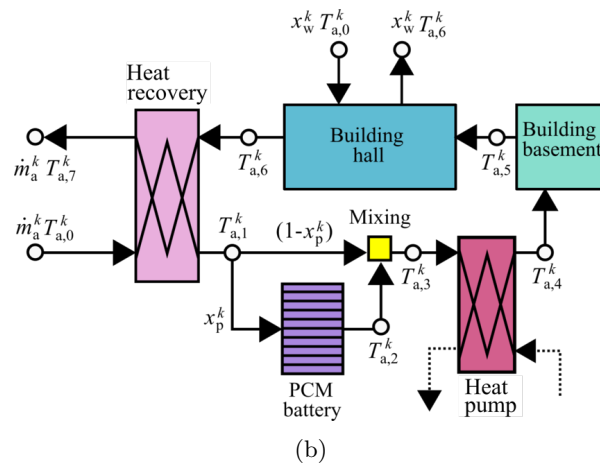
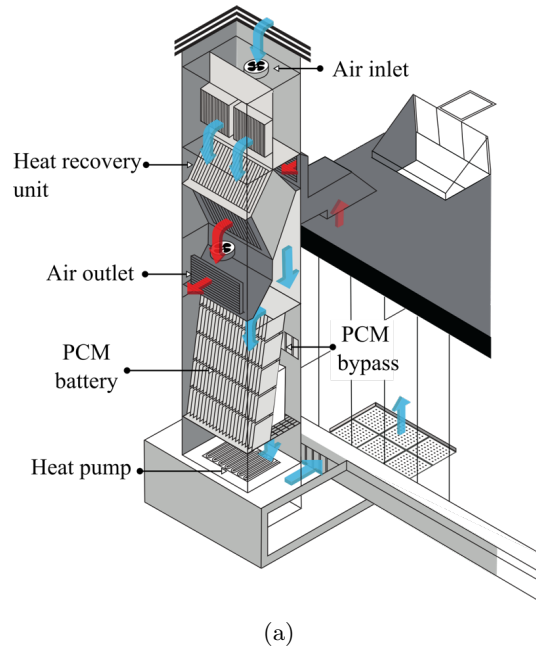


Figure 2: (a) Detail of the climate tower with heat recovery unit and PCM battery; and (b) diagram for heat balance on the airflow inside of the system.

Table 1: Building dimensions and properties considered: specific mass (ρ), specific heat (c), radiative emissivity (ε), transmittance (τ), solar absorptance (α), width (X_1), height (X_2), and length (X_3).

Component	ρ [kg/m ³]	c [J/kg/K]	ε [-]	τ [-]	α [-]	X_1 [m]	X_2 [m]	X_3 [m]
Glazing walls (N & S)	2700	840	0.13	0.78	0.06	13.5	5.2	0.01
Glazing walls (E & W)	2700	840	0.13	0.78	0.06	0.01	5.2	22.5
Ceiling	2000	840	–	–	–	13.5	0.003	22.5
Roof	1050	1800	0.92	–	0.87	13.5	0.004	22.5
Indoor deck	1550	800	–	–	0.16	13.5	0.038	22.5
Concrete floor	2000	840	–	–	–	13.5	0.23	22.5

Table 2: Parameters considered for the PCM battery in the climate tower.

Parameter	Value	Parameter	Value
Number of plates	1690	Specific mass	1000 kg/m ³
Volume of each plate	0.0012 m ³	Specific heat	1400 J/kg/K
Distance between plates	4 mm	Specific latent heat	310000 J/kg
Solid phase, T_{ps}	20 °C	Liquid phase, T_{pl}	23 °C

2.1 Numerical model for the building and the climate tower

To study the system behavior, we formulate a numerical model relying on thermodynamics and heat transfer theories [40, 41]. This model arises from the principle of energy conservation, in which the energy balance in a control volume must be zero.

In this case, when dealing with the air volume, the energy balance amounts to:

$$\dot{m}_a(h_{a,in} - h_{a,out}) + \dot{q}_{gen} = UA(T_a - T_c) + m_a \frac{dh_a}{dt} \quad (1)$$

where \dot{m}_a is the airflow rate, h_a the specific enthalpy of the air, \dot{q}_{gen} the internal heat generation, U the overall heat transfer coefficient, A the heat transfer area, T_a the temperature of the air, T_c the sink temperature, m_a the mass of air in the control volume, and t the time variable. Note that we consider heat as the prevailing energy, disregarding the potential and kinetic energy, while also assuming a fully mixed temperature scenario with no internal stratification. Moreover, even though the air naturally contains water vapor, we aim, for simplicity, at heating and cooling without considering humidification processes (e.g., heating with humidification or cooling with dehumidification) since several configurations could be explored, including liquid desiccant regenerators [42], fan coil units [43], and desiccant packed beds [44], and this is not the purpose of the present study. Hence, the specific enthalpy of the air does not include the latent heat of the moisture, and $h_a = c_{p,a}T_a$.

The diagram for the heat balance over the airflow is shown in Figure 2b, where one can see the blocks for the volumes of interest i.e., for heat recovery (volume 1), PCM battery (volume 2), mixing unit (volume 3), active system (volume 4), building basement (volume 5), and building hall (volume 6). Applying (1) in each volume mentioned, in which the superscript k is the current time step and Δt is the length of the discretization time, the temperatures of the air can be determined as output variables. Therefore, downstream the heat recovery unit we obtain the following expression:

$$T_{a,1}^k - T_o^k = x_r^k \eta (T_{a,6}^k - T_o^k) \quad (2)$$

where T_o^k is the outside air temperature. The symbol η in (1) refers to the heat exchanger efficiency, which, according to the values measured at The Green Village, is here set at $\eta = 80\%$. Moreover, x_r^k is the optimization parameter set as a fraction of 1 for determining the optimal dynamic use of heat recovery. For example, $x_r^k = 1$ means that the heat recovery unit is regarded at full capacity while $x_r^k = 0$ indicates that the heat recovery unit is fully bypassed, while in general x_r^k may continuously vary within the interval $[0, 1]$. Such fraction is here idealized and in practice it could represent, for example, multiple channels with a controllable heat exchanger area. Subsequently, the outlet temperature of the airflow running through the PCM battery ($T_{a,2}^k$) is determined by

$$x_p^k \dot{m}_a^k c_a (T_{a,2}^k - T_{a,1}^k) = h^k A (T_p^k - T_{a,2}^k) \quad (3)$$

where \dot{m}_a^k is the airflow rate, x_p^k is the flow fraction for the PCM battery, h^k the convection coefficient, and T_p^k is the temperature of the plates in the PCM battery. In parallel, the airflow that bypasses the PCM battery $(1 - x_p^k)$ comes across the airflow crossing the PCM battery (x_p^k) in the mixing point shown in Figure 2b, where the mix temperature can be determined as

$$T_{a,3}^k = x_p^k T_{a,2}^k + (1 - x_p^k) T_{a,1}^k \quad (4)$$

Next, the airflow goes through the active system, where the thermal power required for heating or cooling the airflow is determined by

$$\dot{q}_{as}^k = \dot{m}_a^k c_a (T_{a,4}^k - T_{a,3}^k) \quad (5)$$

where $T_{a,4}^k$ is the temperature set to meet the desirable indoor condition at the building hall. Note, however, that the airflow first crosses the building basement before reaching the main hall. The air temperature downstream the building basement $T_{a,5}^k$ is determined as follows:

$$\dot{m}_a^k c_a (T_{a,5}^k - T_{a,4}^k) = h^k A (T_d^k - T_{a,5}^k) + h^k A (T_f^k - T_{a,5}^k) - \frac{m_{a,5} c_a (T_{a,5}^k - T_{a,5}^{k-1})}{\Delta t} \quad (6)$$

where T_d^k is the deck temperature, T_f^k is the basement floor temperature, and m_a is the mass of air. For the air temperature in the building hall, we apply

$$\begin{aligned} \dot{m}_a^k c_a (T_{a,6}^k - T_{a,5}^k) = & x_w^k \rho_a C_d \varphi \sqrt{\frac{2gH |T_{a,6}^k - T_{a,0}^k|}{T_{a,0}^k}} c_a (T_{a,0}^k - T_{a,6}^k) + P^k \dot{q}_p + \sum_{j=1}^6 h^k A (T_{s,j}^k - T_{a,6}^k) \\ & - \frac{m_{a,6} c_a (T_{a,6}^k - T_{a,6}^{k-1})}{\Delta t} \end{aligned} \quad (7)$$

in which x_w^k is the aperture fraction of the sky windows, C_d is the discharge coefficient, φ is the cross-sectional area, g the gravitational acceleration, and H is the height of the sky windows. The building has four sky windows and a total cross-sectional area $\varphi = 12 \text{ m}^2$ while $C_d = 0.62$, which is the discharge coefficient usually assumed. Moreover, P^k is the number of occupants and \dot{q}_p is the heat generation from people: as standard in the literature, we consider an overall value of 110 W per person including the use of electrical devices [45]. Furthermore, $T_{s,j}^k$ refers to the temperature of the indoor surfaces: internal walls ($T_{w,1}^k$), ceiling (T_c^k), and deck (T_d^k).

The system formulation still requires energy balances for determining the temperature of each solid volume coupled to the air volume. Therefore, assuming a lumped-heat capacity, the energy balance for the solid volumes is obtained as follows:

$$\dot{q}_{in} - \dot{q}_{out} = m_s \frac{dh_s}{dt} \quad (8)$$

where \dot{q}_{in} is the heat rate coming into the system, \dot{q}_{out} the heat rate coming out of the system, m_s the solid mass in the volume, and h_s the specific enthalpy of the solid, which is here assumed as $dh_s = c_{p,s} dT_s$. For the triple-glazed walls, we consider the balances from (8) in each facade (i.e., N, S, E, and W), while obtaining the following expressions for internal ($T_{w,1}^k$), central ($T_{w,2}^k$), and external ($T_{w,3}^k$) layers:

$$\frac{m_w c_w (T_{w,1}^k - T_{w,1}^{k-1})}{A \Delta t} = I_w^k \tau_w^2 \alpha_w + h^k (T_{a,6}^k - T_{w,1}^k) + K_w (T_{w,2}^k - T_{w,1}^k) + \frac{\sigma ((T_{w,2}^k)^4 - (T_{w,1}^k)^4)}{\left(\frac{1}{\varepsilon_w} + \frac{1}{\varepsilon_{w,2}} - 1\right)} \quad (9)$$

$$\begin{aligned} \frac{m_w c_w (T_{w,2}^k - T_{w,2}^{k-1})}{A \Delta t} = & I_w^k \tau_w \alpha_w + K_w (T_{w,1}^k - T_{w,2}^k) + K_w (T_{w,3}^k - T_{w,2}^k) \\ & + \frac{\sigma ((T_{w,1}^k)^4 - 2(T_{w,2}^k)^4 + (T_{w,3}^k)^4)}{\left(\frac{1}{\varepsilon_w} + \frac{1}{\varepsilon_{w,2}} - 1\right)} \end{aligned} \quad (10)$$

$$\begin{aligned} \frac{m_w c_w (T_{w,3}^k - T_{w,3}^{k-1})}{A \Delta t} = & I_w^k \alpha_w + K_w (T_{w,2}^k - T_{w,3}^k) + h^k (T_o^k - T_{w,3}^k) \\ & + \frac{\sigma ((T_{w,2}^k)^4 - (T_{w,3}^k)^4)}{\left(\frac{1}{\varepsilon_w} + \frac{1}{\varepsilon_{w,2}} - 1\right)} + \varepsilon_w \sigma ((T_{sky}^k)^4 - (T_{w,3}^k)^4) \end{aligned} \quad (11)$$

where I_w^k is the solar irradiance on the wall, τ is the transmittance, α is the absorptance, σ is the Stefan-Boltzmann constant, and T_{sky} the sky temperature. Note that (7), (8), and (9) consider radiative heat transfer terms, which are proportional to the fourth power of the temperature of the surfaces. Furthermore, we include the heat diffusion in-between the glass layers, which are filled with Argonium, while the radiative heat transfer between the surfaces indoors is neglected, as convective terms are the dominant forces. For the roof and the ceiling, the following pair of equations is considered:

$$\frac{m_r c_r (T_r^k - T_r^{k-1})}{A \Delta t} = I_r^k \alpha_r + h^k (T_o^k - T_r^k) + \varepsilon_r \sigma \left((T_{sky}^k)^4 - (T_r^k)^4 \right) + K_r (T_c^k - T_r^k) \quad (12)$$

$$\frac{m_c c_c (T_c^k - T_c^{k-1})}{A \Delta t} = K_r (T_r^k - T_c^k) + h^k (T_{a,6}^k - T_c^k) \quad (13)$$

where K_r is the conductive coefficient for the thermal isolation at the roof. Similarly, when dealing with the concrete floor and tile deck, the energy balance results in

$$\frac{m_f c_f (T_f^k - T_f^{k-1})}{A \Delta t} = h^k (T_{a,5}^k - T_f^k) + K_f (T_g^k - T_f^k) \quad (14)$$

$$\frac{m_d c_d (T_d^k - T_d^{k-1})}{A \Delta t} = x_s^k I_d^k \tau_w^3 \alpha_d + h^k (T_{a,6}^k - T_d^k) + h^k (T_{a,4}^k - T_d^k) \quad (15)$$

where x_s^k is the aperture fraction of the solar shades and T_g^k the temperature of the ground. In the PCM battery, the energy balance considers the liquid fraction variance [46], which depends on the actual temperature of the plate as follows:

$$\frac{(1 - y_p^k) m_p c_p^k (T_p^k - T_p^{k-1}) + m_p L_p (y_p^k - y_p^{k-1}) + y_p^k m_p c_p^k (T_p^k - T_p^{k-1})}{\Delta t} = h^k A (T_{a,2}^k - T_p^k) \quad (16)$$

where L_p is the specific latent heat, and y_p^k is the liquid fraction during the solid-liquid transition:

$$y_p^k = 1 - \frac{(T_{pl} - T_p^k)}{(T_{pl} - T_{ps})} \quad (17)$$

where T_{pl} is the temperature of the liquid phase and T_{ps} is the temperature of the solid phase.

Regarding the convection coefficients (h^k), we rely on classic correlations that are expressed in terms of the nondimensional Re , Ra , and Pr numbers [40]. For instance, if the air velocity is greater than 0.1 m/s, the following equation is applied to any surface:

$$h^k = \frac{\gamma}{L_c} 0.037 (Re^k)^{0.8} (Pr^k)^{0.33}$$

where L_c is the surface's characteristic length and γ is the thermal conductivity of the air. On the other hand, if the air velocity over the surface is less than 0.1 m/s, a different pair of equations are considered, which depend on the surface orientation. For the vertical surfaces (i.e., walls), the following equations are considered:

$$h^k = \frac{\gamma}{L_c} \left(0.825 + \frac{0.387(Ra^k)^{0.167}}{\left[1 + \left(\frac{0.492}{Pr^k} \right)^{0.562} \right]^{0.296}} \right)^2 \quad \text{if } Ra^k \geq 10^9 \quad (18a)$$

$$h^k = \frac{\gamma}{L_c} \left(0.680 + \frac{0.670(Ra^k)^{0.25}}{\left[1 + \left(\frac{0.492}{Pr^k} \right)^{0.562} \right]^{0.444}} \right) \quad \text{if } Ra^k < 10^9 \quad (18b)$$

while for the horizontal surfaces, such as the roof, ceiling, deck, and concrete floor, the heat transfer coefficient is calculated as follows:

$$h^k = \frac{\gamma}{L_c} 0.54(Ra^k)^{0.25} \quad \text{if } Ra^k \leq 10^7 \quad (19a)$$

$$h^k = \frac{\gamma}{L_c} 0.15(Ra^k)^{0.33} \quad \text{if } Ra^k > 10^7 \quad (19b)$$

Table 3: Dynamic inputs and outputs for the system model.

Inputs	Symbol	Outputs	Symbol
Air mass flow rates	\dot{m}_a^k	Air temp. in the tower	$T_{a,1-4}^k$
Solar irradiance	I^k	Air temp. in the building	$T_{a,5-6}^k$
Outside temperature	T_o^k	Glass temperature	$T_{w,1-3}^k$
Sky windows aperture fraction	x_w^k	Deck temperature	T_d^k
Solar shades aperture fraction	x_s^k	Floor temperature	T_f^k
PCM bypass fraction	x_p^k	Ceiling temperature	T_c^k
Heat recovery fraction	x_r^k	Roof temperature	T_r^k
Building inlet temperature	$T_{a,4}^k$	PCM plate temperature	T_p^k
Number of occupants	P^k	Active thermal power	\dot{q}_{as}^k

However, (19a) and (19b) only apply when the surface is cooling down. When the surface is warming up, the following equation is regarded:

$$h^k = \frac{\gamma}{L_c} 0.27(Ra^k)^{0.25} \quad (19c)$$

For determining the solar incidence over each surface we rely on the method suggested in [47], in which the direct (I_b^k), diffuse (I_d^k), and ground-reflected (I_g^k) radiation are computed individually and the total solar incidence is determined as $I^k = I_b^k + I_d^k + I_g^k$. Therefore,

$$I_b^k = I_{bn}^k \cos(\theta^k) \quad (20)$$

where I_{bn}^k is the direct normal irradiance, and θ^k is the angle of incidence between the ray of sun and the surface normal (see [47] for more details on this calculation). The diffuse component calculations rely on the Perez model [47]:

$$I_d^k = I_{dh}^k \left[(1 - P_1^k) \left(\frac{1 + \cos(\beta)}{2} \right) + P_2^k + P_3^k \sin(\beta) \right] \quad (21)$$

where I_{dh}^k is the diffuse horizontal irradiance on the horizontal plane, β is the surface's inclination angle, and P_1^k , P_2^k and P_3^k are model coefficients [47]. Finally, the ground-reflected radiation is calculated as

$$I_g^k = I_h^k \left(\frac{1 - \cos(\beta)}{2} \right) \xi \quad (22)$$

where I_h^k refers to the global horizontal irradiance and ξ to the ground reflectance.

Table 3 summarizes the main input and output variables considered in the model.

2.2 Numerical validation

All equations were implemented in MATLAB using *fsolve* to determine the temperatures in the nonlinear system of equations (1)–(17) while the thermal-physical properties of the air are obtained from the CoolProp library [48]. To validate the numerical implementation, we compare the model outputs against the measurements collected in situ. The physical system is monitored by a set of Negative Temperature Coefficient (NTC) thermistors, which provide the temperatures and air mass flows for 5-minutes intervals. The specifications of the sensors include a nominal resistance of 10k Ω at 25 °C, an accuracy of 5%, a sensitivity of 1%, and a measuring range between −40 and 105 °C. In total, 53 sensors were considered for the validation, and they are positioned according to Table T4. Note that sensors are uniformly distributed in each space and the average temperature of these sensors is taken as the representative temperature of the corresponding space. Additionally, a local weather station measures global horizontal irradiance, outside temperature, and wind velocity, which are inputs for the current model. In this case, the pyranometer used to measure solar radiation was provided and calibrated by Priva B.V., the manufacturer.

The validation results are presented in Figure 3, considering the measurements collected at The Green Village between April 2–11, 2021. As shown in Figure 3, the temperature profiles suggest fair accordance between the numerical and experimental values, supporting the accuracy of the model. We use the accounted variance as a measure of the accuracy of the model, which ranges between 85% for the deck floor surface and 95% for the indoor air temperature. Considering the simplifications assumed in the modeling (e.g., lumped capacitance and heat transfer correlations) we can judge the overall accuracy of the model as very

Table 4: Positioning of the temperature sensors.

Position	Number of sensors
Indoor air (hall)	3
Glazed facade	10
Ceiling	4
Deck	9
Concrete floor	9
PCM	18

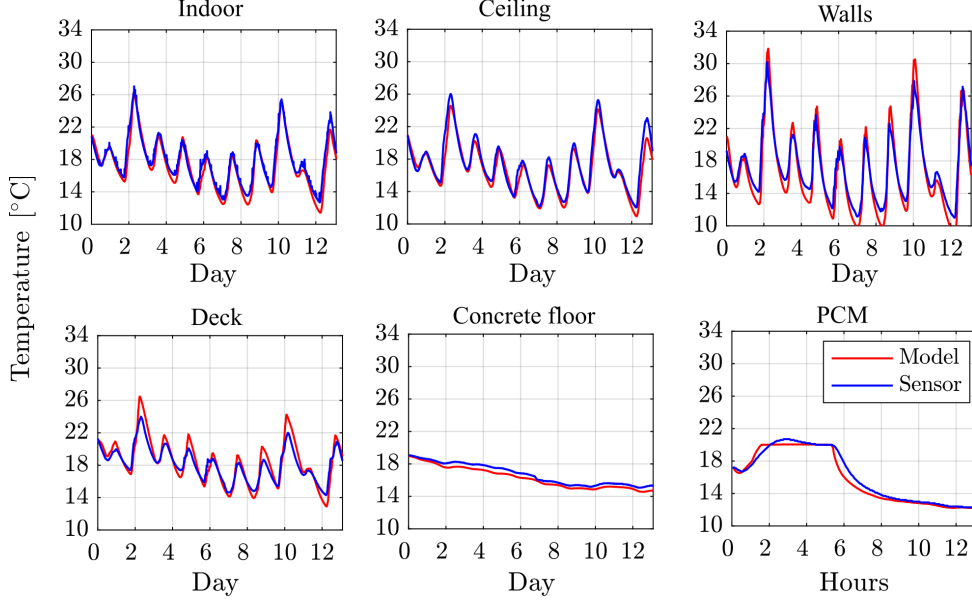


Figure 3: Temperature profiles from the proposed model and the measured data collected at the real building, for (a) indoor air, (b) ceiling, (c) all-glass facades, (d) deck, (e) concrete floor, and (f) phase-change material.

satisfactory. Therefore, this model can be used for meaningful analysis and optimization of the system, as explained in the next section.

3 Optimizing design and operational parameters

The system considered, as presented in Figure 1, and discussed in Section 2, has been designed to operate under variable operation and weather conditions. Since the selected design and operational parameters play a major role in the proper system integration, synchrony, and performance, in this section we optimize the selection of these parameters to find the best set of inputs toward the desired output that is the minimization of the active energy required while meeting the thermal comfort references.

3.1 Weather data and people occupancy

The dynamic optimization considers hourly Typical Meteorological Year (TMY) data provided by the World Meteorological Organization (WMO) for Amsterdam, which is shown in Figure 4. Such data resembles weather conditions for most regions of the Netherlands, including Delft, which is located about 55 km away from Amsterdam. Figure 4 shows the solar irradiances, wind velocity, and ambient temperatures as a function of time (the months of the year are indicated on the x-axis). For instance, the direct normal irradiance values peak between 600 W/m^2 in winter and 900 W/m^2 in summer, as the outside temperature ranges between $-5 \text{ }^\circ\text{C}$ and $35 \text{ }^\circ\text{C}$. Hence, the dataset comprises a wide range of weather conditions.

Regarding the people occupancy, even though the building is designed to host up to 210 people, we consider a daily occupancy of 30 people between 9:00 and 17:00, based on the annual visitation record of The Green Village. During this period, here defined as occupied, the HVAC system must attend to

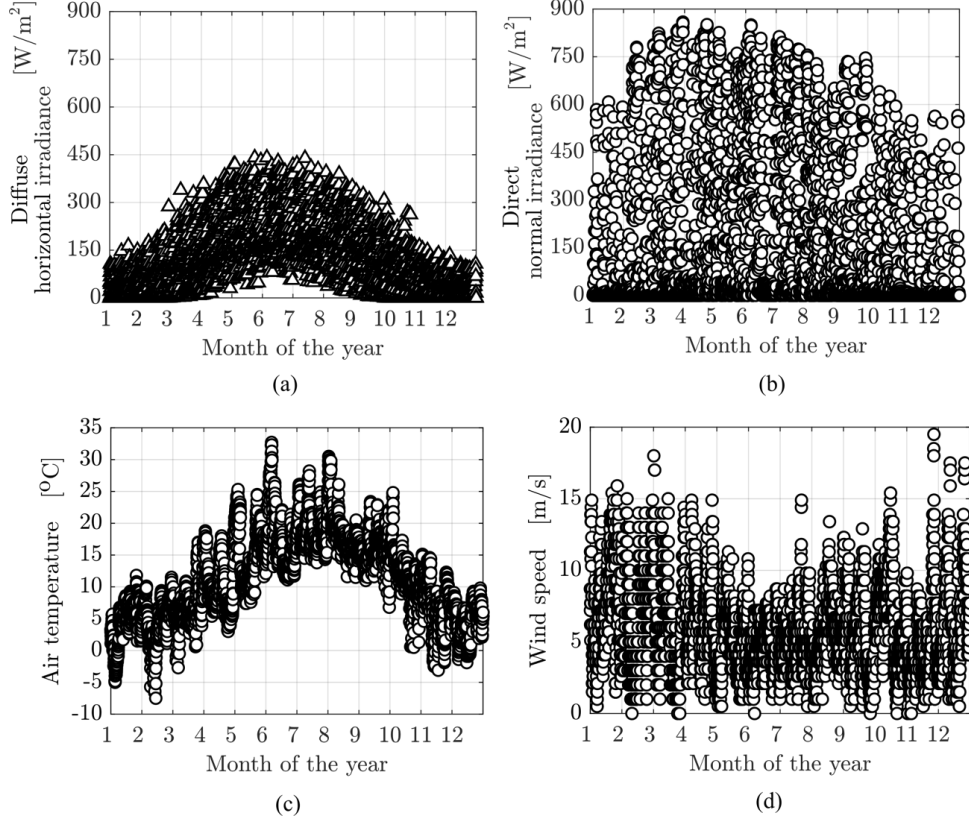


Figure 4: TMY (Typical Meteorological Year) data for Amsterdam, in the Netherlands, with (a) global horizontal irradiance, (b) direct normal irradiance, (c) air temperature, and (d) wind speed.

the reference temperatures established. In the non-occupied period, however, indoor temperatures are not constrained, and this period may be regarded to prepare the building for the next day.

3.2 Optimization formulation

The aim is to identify optimal parameters when operating the HVAC system to meet the desired conditions while minimizing the auxiliary backup use (\dot{q}_{hp}^k), i.e., we consider

$$\min_{\gamma} \sum_{k=1}^N \dot{q}_{\text{hp}}^k \quad (23)$$

in which γ refers to the parameters to be optimized and N is the optimization horizon. In this paper, we regard an optimization horizon of 24 hours while simulating the entire year. Therefore, we perform 365 optimizations in total.

The optimization problem is solved using the SQP (Sequential Quadratic Programming) algorithm of *fmincon*, from MATLAB's optimization toolbox. Furthermore, as the problem (22) is nonconvex, each optimization round considers five different starting points to minimize the probability of ending up in a local minimum. Numerical experiments have shown that using 5 different starting points for each variable being optimized was sufficient.

The design and operational parameters γ selected are the deck heat capacity ($m_d c_d$), the deck solar absorptance (α_d), the air mass flow demand (\dot{m}_a^k), the heat recovery fraction (x_r^k), the PCM utilization (x_p^k), the solar shading aperture (x_s^k), the sky windows aperture (x_w^k), and the building inlet temperature ($T_{a,4}^k$),

which are subjected to the following bounds:

$$0 \leq m_d c_d \leq 4 \cdot E \quad (24a)$$

$$0 \leq \alpha_d \leq 1 \quad (24b)$$

$$0 \leq x_r^k, x_s^k, x_p^k, x_w^k \leq 1 \quad (24c)$$

$$0.1 \text{ kg/s} \leq \dot{m}_a^k \leq 2 \text{ kg/s} \quad (24d)$$

$$10 \text{ }^\circ\text{C} \leq T_{a,4}^k \leq 35 \text{ }^\circ\text{C} \quad (24e)$$

$$20 \text{ }^\circ\text{C} \leq T_{a,6}^k \leq 24 \text{ }^\circ\text{C} \quad \text{if } k \text{ is occupied} \quad (24f)$$

where (24a)–(24e) are input constraints and (24f) is the system output constraint. The symbol E in (24a) refers to the heat capacity in the experiment: $E = 14.25 \text{ MJ/K}$.

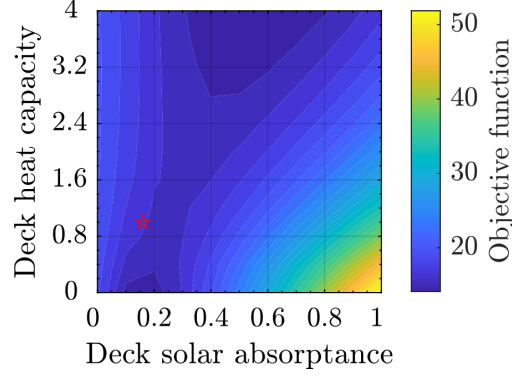
3.3 Evaluating the optimal profiles

Among relevant design parameters, the system’s heat capacity plays an important role in energy conservation for passive systems since different materials provide different heat performances. Although the heat capacitance of all the surfaces could be investigated, the following analysis aims at the numerical optimization of the deck floor due to the special configuration of the building we study, i.e., while in regular buildings the solar heat gain over the walls is typically a key parameter, for the HVAC system design shown in Figure 1 the deck floor heat capacity plays the major role as the transparent walls allow the solar radiation to reach the deck.

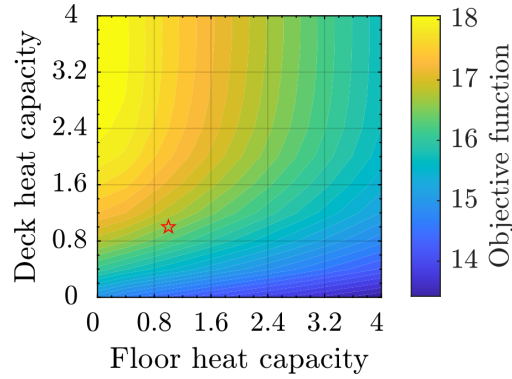
In this sense, the map shown in Figure 5a suggests there is an optimal solar absorptance to minimize the objective function (23) that is dependent on the deck heat capacity. For instance, with a deck heat capacity at 1.6 (i.e., 160% higher than in the original building), the optimal solar absorptance of the simulated system lies between 0.2 and 0.4 - note that the heat capacities in the y-axis are normalized by the heat capacity of the original building (marked by a red star). Considering the blue color range, as most of the area in Figure 5a refers to the blue color, one can observe that the difference between the maximal and minimal heating demand reaches up to 40%. Also, reducing the deck mass could increase the yearly savings by about 12%. The optimal deck floor configuration mostly suggests low heat capacities and low solar absorptance because the internal heat transfer coefficient for cooling on this surface is limited, even though it can be further optimized (e.g., one could use fins or microchannels for enhancing heat transfer). On the other hand, Figure 5b illustrates the effects of increasing the heat capacity of the concrete floor. The heat capacity of the concrete does not to be relevant when the system has a low deck heat capacity since the air heat gains over the deck are dominant. However, higher heat capacities of the concrete floor may become slightly useful (maximum 10% of the energy consumption) when dealing with high deck heat capacities since the increase of floor mass could balance the increase of deck mass. During the optimization of the operational parameters, the heat capacity is constant and equal to the value marked by the red star in Figure 5, while the operational parameters are optimized as explained next.

For assisting the indoor temperature and ventilation, the active system relies on two variables: the air mass flow rates and the air temperature downstream the tower (upstream the building). While the ventilation requirement corresponds to the air quality indoor, the airflow rates also affect the indoor temperature and can be optimized to better control the indoor ambient and to avoid some inconveniences of excessive ventilation such as noise, and more regular replacement of the air filters. In this sense, such optimization considers the limits shown in (24d) while determining the optimal airflow. The optimization results are shown in Figure 6, in which the people occupancy period is divided into two parts: occupied (from 9:00 until 17:00) and non-occupied (from 17:00 until 9:00). Firstly, Figure 6a illustrates the required airflow during the non-occupied period, in which a comfort temperature is not established but the active system must condition the building for the day after. One can note that the airflow demand is higher in the warmer and colder seasons because of the heat exchanges with the environment. Such behavior is sharper at occupied periods (Figure 6b) since the air temperature is restricted in this case.

Following up on the discussion provided for Figure 6, Figure 7 considers the optimization of the air temperatures downstream the tower (i.e., upstream of the building). Recalling that a combination of the heat recovery unit, PCM battery, and active thermal power is considered in the climate tower, as shown in Figure 2a, Figure 7 suggests the optimal air temperatures downstream the tower to meet the desired indoor conditions. This reflects the best match in terms of temperatures and flow rates for the HVAC system with minimal auxiliary use. The results presented in Figure 7 show that the optimal temperatures indicated for summer get close to the reference most of the time (i.e., between 20 °C and 24 °C). In contrast, one can



(a) Deck heat capacity vs. deck solar absorptance



(b) Deck heat capacity vs. floor heat capacity

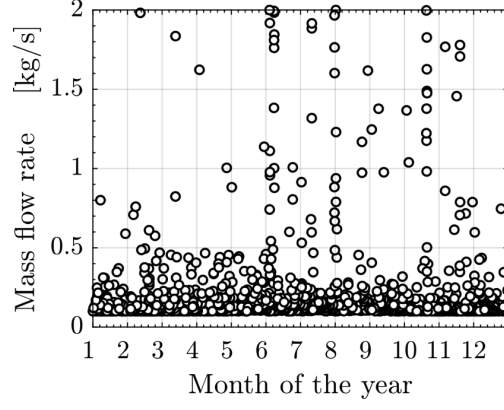
Figure 5: (a) Effect of the deck heat capacity and the solar absorptance on the active demand; and (b) effect of the deck heat capacity and the floor heat capacity on the active thermal demand. The red star points to the values accounted for the real building. The deck heat capacity is expressed as a multiple of the deck heat capacity: 4 means four times the reference. Note that the unit of the objective function is not relevant to the analysis.

note that the larger variation in hourly optimal values occurs in the winter season, which highlights the need for developing operation strategies for such situations. Also, the values provided for optimal temperature indicate references for choosing the substance of PCM and operation points for designing the heat exchangers.

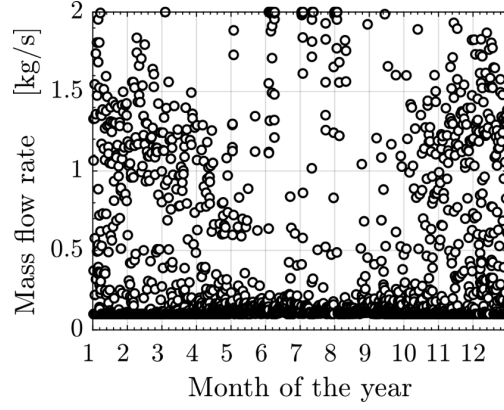
The heat recovery unit installed in the climate tower, which consists of an air-to-air plate heat exchanger with constant effectiveness at 80%, is certainly a key component for saving energy in winter. However, as the outside temperatures increase the system may require temperatures colder than the ones downstream the heat recovery. Figure 8, therefore, explores the optimal use of this heat recovery process over the year. As one can see, in summer often part of the capacity of the heat recovery unit is required, including months in which no heat recovery is required (e.g., between months 5–6 and 7–8). Also, such a period demands more attention since the variable operational range, in this case, is larger than in winter, when the heat recovery is mostly used at full capacity.

Next, we consider the optimization of the PCM battery as an operational parameter to minimize the auxiliary heating while making the building inlet temperature closer to the optimal values determined in Figure 7. PCMs have been suggested for improving energy efficiency in buildings, such as minimizing heat losses by delaying the temperature increase over the external walls or by increasing the stack effect by a temperature enhancement downstream the thermal chimneys, even though the usage of PCM in buildings is still rare. In this paper, the PCM battery is treated as a thermal buffer that passively damps the temperature oscillations of the air outside the building. Recalling the present configuration (Figure 2a), one should note that the lower half of the tower is embedded with a PCM battery composed of several plates arranged along the flow area.

The following analysis starts by exploring the optimal bypass fraction through the PCM battery (x_p^k) to



(a) Non-occupied period



(b) Occupied period

Figure 6: Optimal airflow rates for operating the HVAC system.

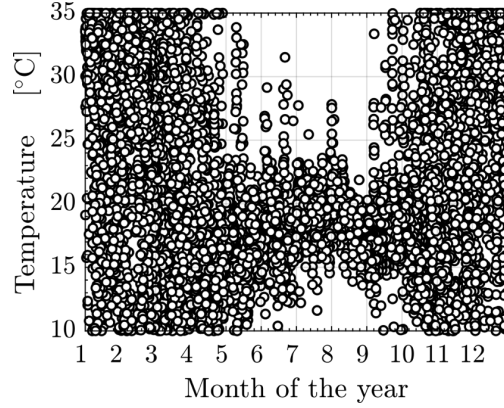


Figure 7: Optimal air temperatures targeted by the climate tower.

minimize the auxiliary heating power, by selecting the best periods during which the airflow passes through the PCM battery; the flow rate coming into the tower can then be split with a fraction x_p^k which is varying continuously from 0 to 1, where $x_p^k = 1$ indicates to pass all the air flowing through the PCM plates and $x_p^k = 0$ means to by-pass the PCM battery. Such analysis regards the volume occupied by the PCM plates connected in parallel as shown in Figure 2a, where there is a 4 mm space between two plates. In total, 1690 plates were considered. The PCM considered is Calcium Chloride Hexahydrate ($\text{CaCl}_2 \cdot 6\text{H}_2\text{O}$), which has been considered for latent storage in buildings [49], providing a specific heat of fusion $L_p = 310\,000$ J/kg. Parameters for dimensions and other properties of the PCM plates are listed in Table 2.

Figure 9a illustrates the optimal values for x_p^k , which suggest a high distribution of fractions all over the

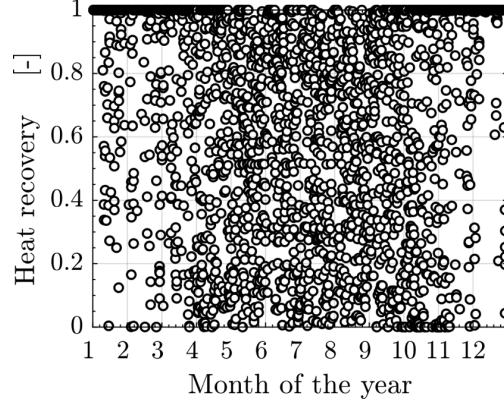
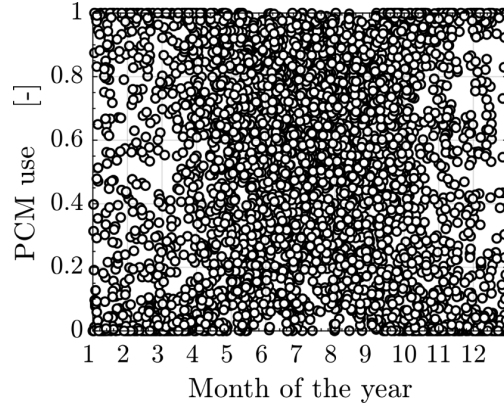
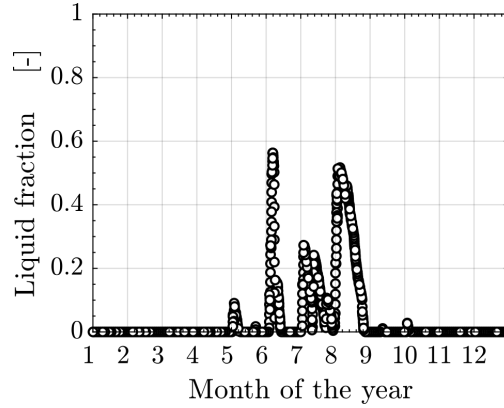


Figure 8: Optimal utilization of the heat recovery unit.



(a) PCM utilization



(b) Liquid fraction

Figure 9: (a) Optimal PCM utilization profile and (b) liquid fraction of the PCM.

year. More precisely, the winter season is characterized by a higher oscillation between periods of use which include full and no flow rates through the PCM battery. Moreover, during the winter there is no phase change in the battery, as shown in Figure 9b, as the system relies only on the sensible heat storage of PCM for thermal buffering. This is because the heat source to charge the PCM is the outside air, so during the winter, there is no phase change and, therefore, less buffering. On the other hand, bypassing the airflow rate through the PCM battery is most evident in summer seasons, where an optimal range of 0.3–0.8 can be noted, while reasonable phase changes at 0.5–0.6 of the maxima are observed. The results indicate that the material used to build the PCM affects the system dynamics. In this sense, a PCM battery comprising different types of materials could be used and controlled for operation over the year.

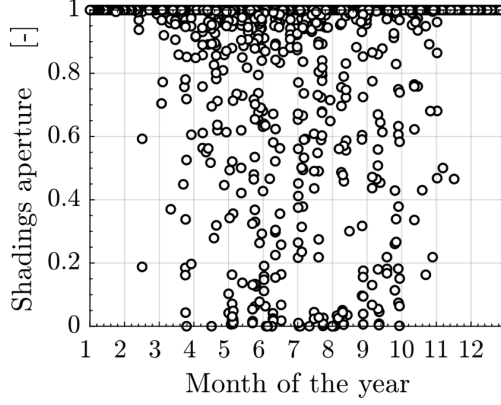


Figure 10: Optimal aperture fractions for solar shadings.

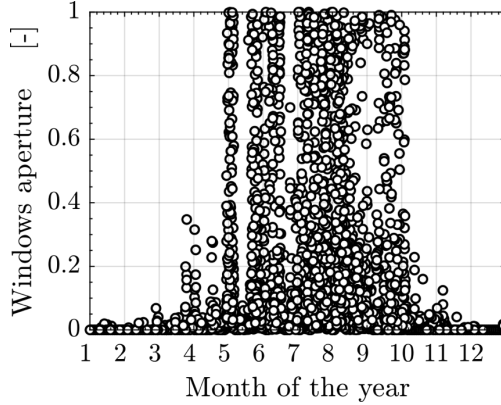


Figure 11: Optimal aperture fractions of sky windows.

When focusing on the optimization of passive technologies, the analysis proceeds considering the dynamical operation of the aperture fraction x_s^k of the solar shadings as this is the main variable that can be controlled to minimize the auxiliary heat demand. This behavior depends on the weather conditions since a cold season requires incoming heat while a warm season requires shading for cooling. Figure 10 shows the hourly optimal input values for the shading aperture during the months of the year, where one can see that the shadings are kept fully closed only for a couple of hours around summer (i.e., months 6, 7, and 8) while they are kept fully open most of the time in the colder periods, reflecting the heating demand instead of cooling. Moreover, even in warmer periods, the shading usually only blocks part of the radiation, which suggests an optimal operation range of aperture that can be further studied for such weather conditions. In these periods the development of an optimal control strategy that provides the signals to regulate the shades is most crucial. Such periods are located from month 4 to month 10, especially during the transitions between cold and warm seasons (and vice versa).

Finally, the sky windows (see Figure 1a) are another feature of the current system that can have their use optimized. While mostly designed with a focus on night ventilation (i.e., non-occupied periods) and on warmer periods, Figure 11 shows the optimal aperture fraction over the year. As shown, there is significant use of sky windows in the warmer months (6–9) while the maximal aperture is rarely considered. In this case, the optimal system relies on natural ventilation for cooling the building. Also, for night ventilation, only a small fraction of aperture is recommended in winter – the roof windows could also be used for ventilation in general, with no purpose of cooling or heating, which may reduce the energy required by the fans.

4 Discussion on the long-term performance

Having considered the optimization above, the analysis is concluded by considering the long-term performance of the HVAC system. Figure 12 illustrates the average indoor air temperatures provided by the HVAC system during occupied and non-occupied periods. As shown, the indoor temperatures during the occupied periods are strictly kept under the reference range throughout the year. Figure 12 additionally shows the

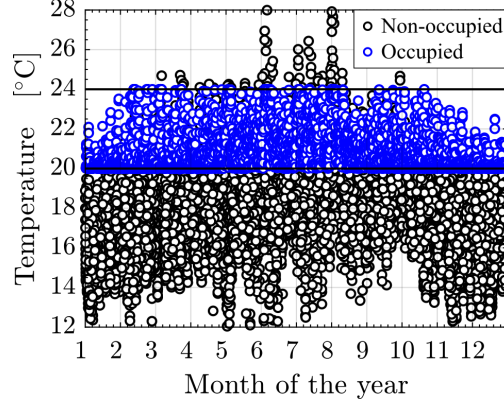


Figure 12: Resulting indoor air temperatures for occupied and non-occupied periods.

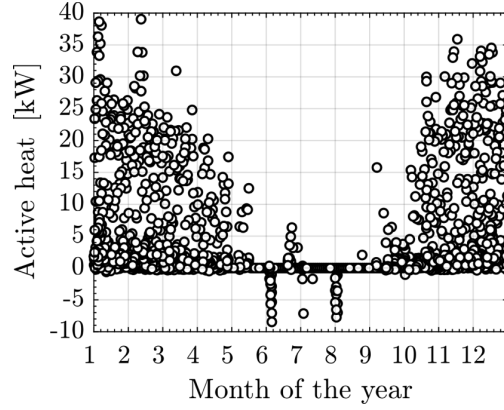
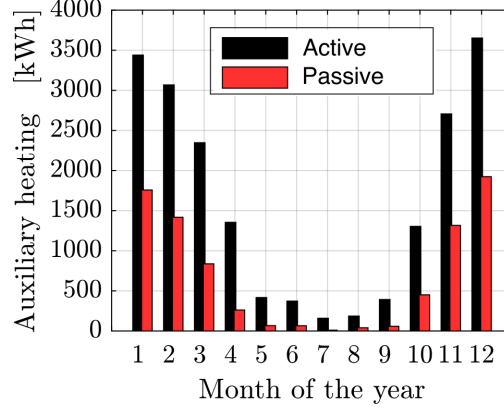


Figure 13: Hourly active demand.

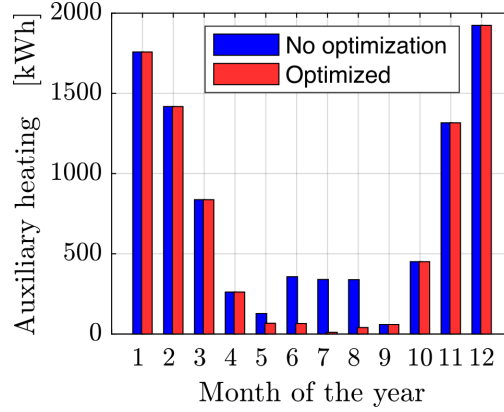
optimal air temperature during the non-occupied period. As one can see, during winter the air temperature indoor is significantly warmer than the outside temperature, which reveals the need to warm up the building for the next day during non-occupied periods. In the warmer months, this difference is reduced.

To illustrate the demand for heating and cooling, Figure 13 presents the hourly thermal input required by the active system over the year. As one can see in Figure 13, the active system operates with higher energy consumption in the cold seasons when it usually requires 20-25 kWh in an hour. Additionally, one can note the heat demand during the non-occupied hours with a concentration of markers at the bottom of Figure 13. In summer, however, the demand is nearly zero (months 6-9). The negative values in Figure 13 indicate a cooling demand that only shows up at some hours in months 6 and 8 and at the same magnitude as for night heating in winter (about 8 kWh in an hour). This demonstrates the prevalence of heating requirements all over the year.

Figure 14a shows the monthly input required for heating and cooling when using solely the active system and when also considering the passive technologies studied (i.e., heat recovery, PCM battery, sky windows, and solar shadings). As shown, the passive sources significantly reduce the active demand in winter while in summer they allow the system to operate with nearly zero-energy consumption as the active demand is also minimized during this period. On a yearly average, passive technologies can supply 58% of the total heating and cooling demand for indoor climate while the heating challenge lies in the low solar incidence levels and outside temperatures. In absolute values, the heat demand for heating and cooling peaks at 27 kWh/m²/year and represents a good trend toward zero-energy buildings. The analysis is concluded in Figure 14b by evaluating the contribution of the optimization of the passive technologies. Figure 14b demonstrates that the optimization of passive sources is effective in summer, while in winter it does not affect the demand since the static system is the best operational approach in this case. In percentual terms, the optimization of the passive sources provides a saving of 10.6% on the total annual heat demand. The yearly contribution obtained is summarized in Table 5.



(a) Effect of passive energy on the total heat consumption



(b) Effect of optimal operation of passive energy technologies

Figure 14: (a) Monthly demand for heating and cooling with active and passive systems, and (b) effect of optimization on passive energy technologies.

Table 5: Yearly passive fractions and auxiliary energy for the cases analyzed.

Cases	Passive fraction [%]	Auxiliary demand [kWh/year]
Active sources optimized and passive system fully closed	0	19 398
Active sources optimized and passive system static	53	9187
Active sources and passive system optimized simultaneously	58	8207

5 Conclusions and future work

This paper has investigated an innovative HVAC system installed in The Green Village with the purpose to explore new technologies and strategies for efficient passive systems. The system uses a combination of a heat recovery unit, PCM buffer, sky windows, and steerable solar shades to provide comfortable temperatures and save energy while assisted by an auxiliary backup. We have proposed a system optimization, which relies on implicit dynamic models and constrained optimization algorithms, to maximize the passive fractions while evaluating the best combination of technologies (i.e., heat exchangers, solar shades, sky windows, and PCM battery).

A study of long-term operation was conducted via optimization procedures for maximizing passive utiliza-

tion, while exploring dynamic features inherent to the system, such as buoyancy, solid heat capacities, and solar irradiance. In this sense, the analysis has identified optimal design parameters and optimal operational conditions for which the indoor environment produced best matches the desired reference temperature, minimizing, therefore, the auxiliary demand. The results clearly showed that while passive systems inevitably depend on variable weather conditions, there are favorable conditions for increasing the system performance, e.g., dynamic scheduling in winter and summer, relevant floor capacity, the combination of temperature and flow rates, etc. The optimization prioritizes passive energy sources and provides control inputs to manage the environment effectively all year round: feedback on maximum loads attained, expected performance, parameter effects, and highest demand time have been reported, which are essential information for optimal design and optimal management.

Finally, the analysis shows that the combination of technologies, when operated optimally, can provide up to 58% of the yearly demand passively, while solar irradiance and heat exchangers have proven to be the most effective component to be managed. Therefore, the system integration we studied demonstrates significant benefits when combining such components and operating them in a synchronized, optimal way. In this sense, further work has been planned considering the development of an optimal schedule for people occupancy, the development of an adaptive comfort strategy with dynamic references for temperature and flow rate, and the development of an optimization approach to maximize the performance of the active system.

Acknowledgments

This work was partly supported by the Netherlands Enterprise Agency (RVO.nl), under the program TKI Urban Energy, grant CONVERGE, by the Research Fund for International scientists, grant 62150610499, by the Key Intergovernmental Special Fund of National Key Research and Development Program, grant 2021YFE098700, and by the Natural Science Foundation of China, grant 62073074.

References

- [1] WHO Regional Office for Europe, “Combined or multiple exposure to health stressors in indoor built environments,” World Health Organization Regional Office for Europe, Copenhagen, 2014.
- [2] S. K. Wang, Handbook of Air Conditioning and Refrigeration, United States: McGraw-Hill, 2001.
- [3] YouGov, “The indoor generation: The effects of modern indoor living on health, wellbeing and productivity,” VELUX Press, Copenhagen, 2018.
- [4] F. J. Kelly and J. C. Fussell, “Improving indoor air quality, health and performance within environments where people live, travel, learn and work,” *Atmospheric Environment*, pp. 90–109, 2019.
- [5] M. Coccia, “Factors determining the diffusion of COVID-19 and suggested strategy to prevent future accelerated viral infectivity similar to COVID,” *Science of the Total Environment*, p. 138474, 2020.
- [6] H. Lia, X.-L. Xu, D.-W. Dai, Z.-Y. Huang, Z. Maa and Y.-J. Guan, “Air pollution and temperature are associated with increased COVID-19 incidence: A time series study,” *International Journal of Infectious Diseases*, pp. 278–282, 2020.
- [7] L. Asere and A. Blumberga, “Does energy efficiency-indoor air quality dilemma have an impact on the gross domestic product?” *Journal of Environmental Management*, p. 110270, 2020.
- [8] X. Cao, X. Dai and J. Liu, “Building energy-consumption status worldwide and the state-of-the-art technologies for zero-energy buildings during the past decade,” *Energy and Buildings*, pp. 198–213, 2016.
- [9] W. Feng, Q. Zhang, H. Ji, R. Wang, N. Zhou, Q. Ye, B. Hao, Y. Li, D. Luo and S. S. Y. Lau, “A review of net zero energy buildings in hot and humid climates: Experience learned from 34 case study buildings,” *Renewable and Sustainable Energy Reviews*, p. 109303, 2019.
- [10] M. Azaza, D. Eriksson and F. Wallin, “A study on the viability of an on-site combined heat- and power supply system with and without electricity storage for office building,” *Energy Conversion and Management*, p. 112807, 2020.
- [11] A. Arabkoohsar, A. Behzadi and A. S. Alsagri, “Techno-economic analysis and multi-objective optimization of a novel solar-based building energy system; An effort to reach the true meaning of zero-energy buildings,” *Energy Conversion and Management* 232, p. 113858, 2021.
- [12] Z. Liu, G. Fan, D. Sun, D. Wu, J. Guo, S. Zhang, X. Yang, X. Lin and L. Ai, “A novel distributed energy system combining hybrid energy storage and a multi-objective optimization method for nearly zero-energy communities and buildings,” *Energy* 239, p. 122577, 2022.

- [13] P. Congedo, C. Baglivo and L. Carrieri, "Application of an unconventional thermal and mechanical energy storage coupled with the air conditioning and domestic hot water systems of a residential building," *Energy and Buildings*, p. 110234, 2020.
- [14] G. Gholamibozanjani and M. Farid, "A comparison between passive and active PCM systems applied to buildings," *Renewable Energy* 162, pp. 112–123, 2020.
- [15] B. C. Zhao and R. Z. Wang, "Perspectives for short-term thermal energy storage using salt hydrates for building heating," *Energy* 189, p. 116139, 2019.
- [16] S. M. Salih, J. M. Jalil and S. E. Najim, "Experimental and numerical analysis of double-pass solar air heater utilizing multiple capsules PCM," *Renewable Energy* 143, pp. 1053–1066, 2019.
- [17] S. Yan, M. A. Fazilati, D. Toghraie, M. Khalili and A. Karimipour, "Energy cost and efficiency analysis of greenhouse heating system enhancement using phase change material: An experimental study," *Renewable Energy* 170, pp. 133–140, 2021.
- [18] H. Huo, W. Xu, A. Li, Y. Lv and C. Liu, "Analysis and optimization of external venetian blind shading for nearly zero-energy buildings in different climate regions of China," *Solar Energy* 223, pp. 54–71, 2021.
- [19] D. de Loyola Ramos Garcia and F. O. Ruttkay Pereira, "Method application and analyses of visual and thermal-energy performance prediction in offices buildings with internal shading devices," *Building and Environment* 198, p. 107912, 2021.
- [20] H. Kim and M. J. Clayton, "A multi-objective optimization approach for climate-adaptive building envelope design using parametric behavior maps," *Building and Environment* 185, p. 107292, 2020.
- [21] Z. Luo, C. Sun, Q. Dong and J. Yu, "An innovative shading controller for blinds in an open-plan office using machine learning," *Building and Environment* 189, p. 107529, 2021.
- [22] G. Zhu and T. -T. Chow, "Design optimization and two-stage control strategy on combined cooling, heating and power system," *Energy Conversion and Management* 199, p. 111869, 2019.
- [23] H. Sobhani, F. Shahmoradi and B. Sajadi, "Optimization of the renewable energy system for nearly zero energy buildings: A future-oriented approach," *Energy Conversion and Management* 224, p. 113370, 2020.
- [24] R. Wang, S. Lu and W. Feng, "A three-stage optimization methodology for envelope design of passive house considering energy demand, thermal comfort and cost," *Energy* 192, p. 116723, 2020.
- [25] F. Robic, D. Micallef, S. P. Borg and B. Ellul, "Implementation and fine-tuning of the Big Bang-Big Crunch optimisation method for use in passive building design," *Building and Environment* 173, p. 106731, 2020.
- [26] S. -H. Park, Y. -S. Jang and Y. -S. K. E. -J. Jang, "Multi-objective optimization for sizing multi-source renewable energy systems in the community center of a residential apartment complex," *Energy Conversion and Management* 244, p. 114446, 2021.
- [27] O. Mahian, M. Javidmehr, A. Kasaeian, S. Mohasseb and M. Panahi, "Optimal sizing and performance assessment of a hybrid combined heat and power system with energy storage for residential buildings," *Energy Conversion and Management* 211, p. 112751, 2020.
- [28] G. S. Georgiou, P. Christodoulides and S. A. Kalogirou, "Optimizing the energy storage schedule of a battery in a PV grid-connected nZEB using linear programming," *Energy* 208, p. 118177, 2020.
- [29] S. Mazzoni, J. Y. Sze, B. Nastasi, S. Ooi, U. Desideri and A. Romagnoli, "A techno-economic assessment on the adoption of latent heat thermal energy storage systems for district cooling optimal dispatch & operations," *Applied Energy* 289, p. 116646, 2021.
- [30] Q. A. Phan, T. Scully, M. Breen and M. D. Murphy, "Determination of optimal battery utilization to minimize operating costs for a grid-connected building with renewable energy sources," *Energy Conversion and Management* 174, pp. 157–174, 2018.
- [31] G. Bianchini, M. Casini, D. Pepe, A. Vicino and G. G. Zanvettor, "An integrated model predictive control approach for optimal HVAC and energy storage operation in large-scale buildings," *Applied Energy* 240, pp. 327–340, 2019.
- [32] B. Vand, R. Ruusu, A. Hasan and B. M. Delgado, "Optimal management of energy sharing in a community of buildings using a model predictive control," *Energy Conversion and Management* 239, p. 114118, 2021.
- [33] S. Yang, M. P. Wan, B. F. Ng, S. Dubey, G. P. Henze, W. Chen and K. Baskaran, "Model predictive control for integrated control of air-conditioning and mechanical ventilation, lighting and shading systems," *Applied Energy* 297, p. 117112, 2021.
- [34] N. S. Raman, K. Devaprasad, B. Chen, H. A. Ingley and P. Barooah, "Model predictive control for energy-efficient HVAC operation with humidity and latent heat considerations," *Applied Energy* 279, p. 115765, 2020.
- [35] J. Reynolds, Y. Rezgui, A. Kwan and S. Piriou, "A zone-level, building energy optimisation combining an artificial neural network, a genetic algorithm, and model predictive control," *Energy* 151, pp. 729–739, 2018.

- [36] Z. Afroz, G. Shafiullah, T. Urmee, M. Shoeb and G. Higgins, “Predictive modelling and optimization of HVAC systems using neural network and particle swarm optimization algorithm,” *Building and Environment* 209, p. 108681, 2022.
- [37] M. Porowski, “The optimization method of HVAC system from a holistic perspective according to energy criterion,” *Energy Conversion and Management* 181, pp. 621–644, 2019.
- [38] X. Wang, v. Cai and X. Yin, “A global optimized operation strategy for energy savings in liquid desiccant air conditioning using self-adaptive differential evolutionary algorithm,” *Applied Energy* 187, pp. 410–423, 2017.
- [39] Y. Jiang, X. Wang, H. Zhao, L. Wang, X. Yin and L. Jia, “Dynamic modeling and economic model predictive control of a liquid desiccant air conditioning,” *Applied Energy* 259, p. 114174, 2020.
- [40] T. L. Bergman, A. S. Lavine, F. P. Incropera and D. P. Dewitt, *Fundamentals of Heat and Mass Transfer*, New York: John Wiley & Sons, 2011.
- [41] A. Bejan, *Advanced Engineering Thermodynamics*, New Jersey: John Wiley & Sons, 2016.
- [42] X. Yin, X. Wang, X. Wei, H. Zhao, L. Wang and L. Jia, “Mathematical model and energy efficiency analysis of a vacuum-based liquid desiccant regenerator,” *Building and Environment* 192, p. 107629, 2021.
- [43] J. Ye, X. Liu, L. Xu and L. Ni, “Experimental study on the heating and humidifying performance of fan coil units with humidification modules in severe cold regions,” *Energy and Buildings* 276, p. 112500, 2022.
- [44] S. D. Antonellis, L. Colombo, A. Freni and C. Joppolo, “Feasibility study of a desiccant packed bed system for air humidification,” *Energy* 214, p. 119002, 2021.
- [45] X. Li and J. Wen, “Review of building energy modeling for control and operation,” *Renewable and Sustainable Energy Reviews*, p. 517–537, 2014.
- [46] R. Vargas-López, I. H.-P. J. Xamán, J. Arce, I. Zavala-Guillén, M. Jiménez and M. Heras, “Mathematical models of solar chimneys with a phase change material for ventilation of buildings: A review using global energy balance,” *Energy*, pp. 683–708, 2019.
- [47] J. A. Duffie and W. A. Beckman, *Solar Engineering of Thermal Processes*, New York: John Wiley & Sons, 2013.
- [48] I. H. Bell, J. Wronski, S. Quoilin and V. Lemort, “Pure and pseudo-pure fluid thermophysical property evaluation and the open-source thermophysical property library CoolProp,” *Industrial & Engineering Chemistry Research*, pp. 2498–2508, 2014.
- [49] V. Tyagi and D. Buddhi, “Thermal cycle testing of calcium chloride hexahydrate as a possible PCM for latent heat storage,” *Solar Energy Materials & Solar Cells*, vol. 92, pp. 891–899, 2008.
- [50] R. W. Fox, A. T. McDonald and P. J. Pritchard, *Introduction to fluid mechanics*, New Jersey: Hoboken, 2008.